Nanoparticles | Hot Paper |

Stable Polymer Nanoparticles with Exceptionally High Drug Loading by Sequential Nanoprecipitation

Yun Liu, Guangze Yang, Thejus Baby, Tengjisi, Dong Chen, David A. Weitz,* and Chun-Xia Zhao*

Abstract: *Poor solubility often leads to low drug efficacy. Encapsulation of water-insoluble drugs in polymeric nanoparticles offers a solution. However, low drug loading remains a critical challenge. Now, a simple and robust sequential nanoprecipitation technology is used to produce stable drug-core polymer-shell nanoparticles with high drug loading (up to 58.5 %) from a wide range of polymers and drugs. This technology is based on tuning the precipitation time of drugs and polymers using a solvent system comprising multiple organic solvents, which allows the formation of drug nanoparticles first followed by immediate precipitation of one or two polymers. This technology offers a new strategy to manufacture polymeric nanoparticles with high drug loading having good long-term stability and programmed release and opens a unique opportunity for drug delivery applications.*

Introduction

Engineering nanoparticles to deliver therapeutic drugs remains an exciting concept. A plethora of nanoparticles (NPs) have been designed to exhibit desirable physicochemical properties for enhanced delivery efficiency.[1] Biodegradable polymeric NPs have been extensively explored as promising drug delivery vehicles owing to their excellent biodegradability and biocompatibility.[2] However, among various polymeric nanoparticle systems, drug loading (the mass fraction of drug in the entire drug-loaded NPs) is usually below 10 %,[3] which hinders their practical applications.

Emulsion-based techniques[4] and nanoprecipitation[5] are two commonly used methods for producing drug-loaded polymeric NPs. Compared to the emulsion methods, nano-

[*] Y. Liu, G. Yang, T. Baby, Tengjisi, C.-X. Zhao
Australian Institute for Bioengineering and Nanotechnology, University of Queensland
St. Lucia, Queensland 4072 (Australia)
E-mail: z.chunxia@uq.edu.au

D. Chen
Institute of Process Equipment, College of Energy Engineering, Zhejiang University
Hangzhou, Zhejiang 310027 (China)

D. Chen, D. A. Weitz
John A. Paulson School of Engineering and Applied Sciences, Harvard University
Cambridge, MA 02138 (USA)
E-mail: weitz@seas.harvard.edu

Supporting information and the ORCID identification number(s) for the author(s) of this article can be found under:
https://doi.org/10.1002/anie.201913539.

precipitation is simpler, more cost-effective and requires no external energy input (for example, homogenization, sonication).[5] However, nanoprecipitation under slow mixing often leads to the failure of drug encapsulation with drug loading less than 5 or even 1 %[6] owing to their different solubility thus different precipitation times. One approach to improve drug loading is to modify the drug or polymer[7] to enhance polymer–drug interactions. Another approach is to use rapid mixing to co-precipitate the drug and polymer, for example, flash nanoprecipitation[8] or microfluidic flow-focusing.[9] However, drug-loaded nanoparticles using such rapid-mixing methods are unstable due to Ostwald ripening and drug recrystallisation especially for those molecules with a water-octanol partition coefficient below 6 (for example, curcumin, paclitaxel).[8c]

Results and Discussion

We report a simple, rapid, and robust nanoprecipitation approach to produce drug-core polymer-shell nanoparticles with exceptionally high drug loading from a wide range of polymers and drugs. Instead of using rapid mixing to co-precipitate the drug and polymer, we tune their solubility by screening different solvent systems and engineering the precipitation process so that the drug can precipitate first followed by immediate precipitation of the polymer. To demonstrate how our method works differently from the traditional nanoprecipitation process, we used a generic hydrophobic drug, curcumin, and shellac (E904, the food additive code), a natural resin which has been used in pharmaceuticals and food industries.[10] For the traditional nanoprecipitation, curcumin and shellac are co-dissolved in a solvent (for example, dimethylformamide (DMF)). Then this solution is added to a large amount of water or buffer with vigorous mixing (Figure 1a). The solution became cloudy instantly and then big aggregates were observed after a few minutes (Figure 1a). Transmission electron microscope (TEM) images show a mixture of polymer nanoparticles and curcumin crystals (Figure 1a; Supporting Information, Figure S1). Because of the intrinsic solubility difference of the drug and the polymer in a single solvent, their precipitation times can be very different, resulting in the formation of large drug aggregates and polymeric nanoparticles containing a very small amount of drug.
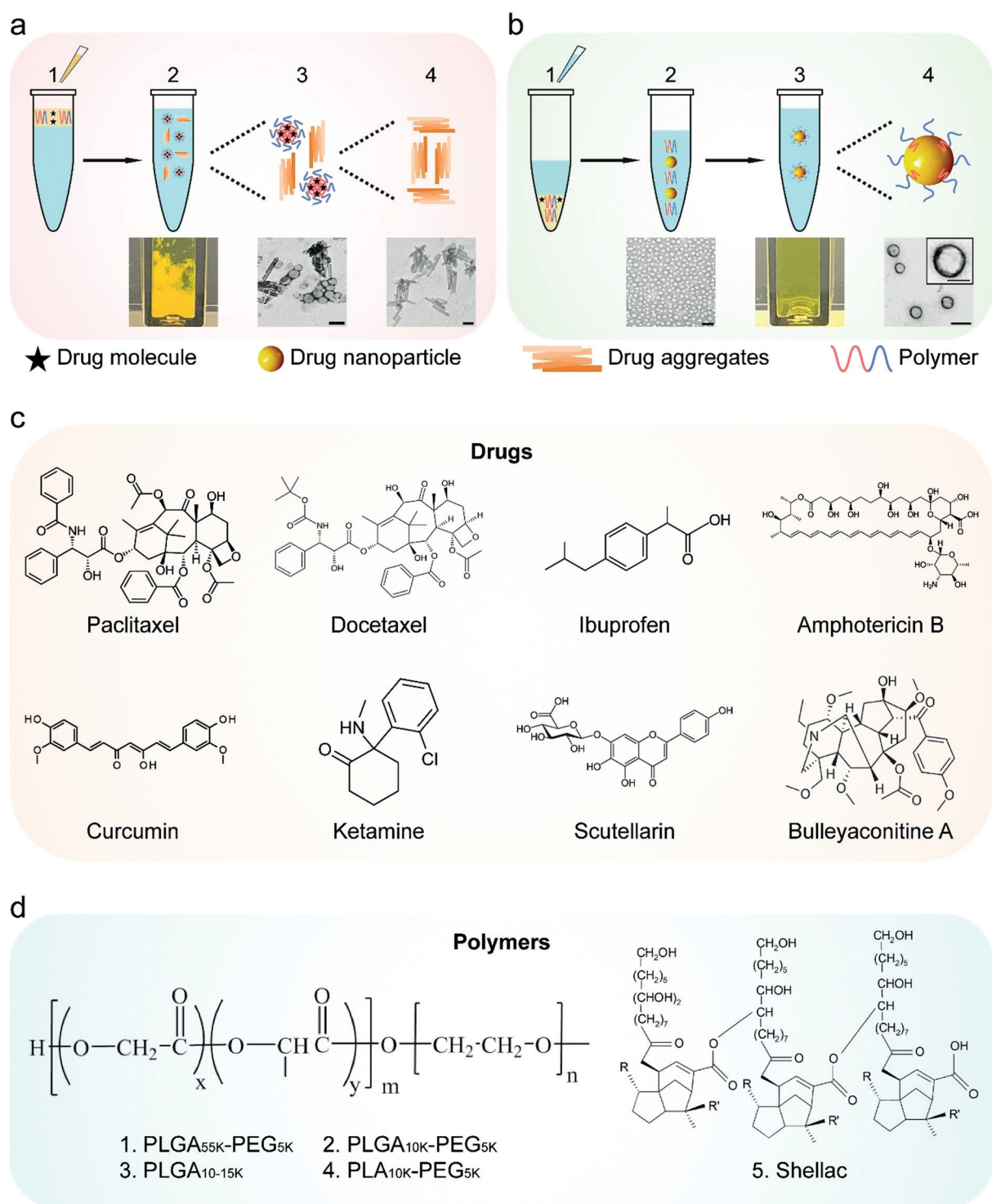
Our nanoprecipitation approach is to use a mixture of multiple solvents (Figure 1b) instead of a single solvent. For example, curcumin and shellac are first dissolved in a solvent

Figure 1. Traditional method and our new nanoprecipitation method. a) The traditional nanoprecipitation method. A solvent solution containing a hydrophobic drug and a polymer is added to an anti-solvent (**1**). Yellow precipitation is observed (**2**) showing a mixture of polymeric NPs and drug crystals (**3**), and enlarged image of drug crystals (**4**). b) Our new nanoprecipitation approach. An anti-solvent is added to a three-solvent mixture containing a hydrophobic drug and a polymer under gentle mixing (**1**). Uniform drug NPs precipitate first (**2**), followed by the precipitation of polymer covering the drug NPs, thus forming a drug-core polymer-shell structure. A homogeneous yellow suspension is observed indicating the complete encapsulation of drug in polymeric nanoparticles (**3**), and the TEM image shows uniform NPs with a core–shell structure (**4**). c) Drugs that we tested for making polymeric nanoparticles with high drug loading including paclitaxel, docetaxel, ibuprofen, amphotericin B, curcumin, ketamine, scutellarin and bulleyaconitine A. d) The polymers we used to encapsulate drugs, including PLGA$_{55K}$-PEG$_{5K}$, PLGA$_{10K}$-PEG$_{5K}$, PLGA$_{10-15K}$, PLA$_{10K}$-PEG$_{5K}$, and shellac. Curcumin and shellac are used to demonstrate the new nanoprecipitation method.

mixture of dimethyl sulfoxide (DMSO), DMF and ethanol (EtOH) at a volume ratio of DMSO/DMF/EtOH = 4:3:3 at the same concentration of 3 mg mL^{-1}. Equal volume of phosphate buffered saline (PBS) buffer at pH 7.4 is poured into this solution with gentle mixing, and uniform curcumin nanoparticles of about 40 nm are observed (Figure 1b). Then another equal volume of the buffer is added resulting in the formation of a homogeneous yellow suspension (Figure 1b) with uniform nanoparticles containing a drug-core and a polymer-shell (Figure 1b). Remarkably, an extremely high drug loading of 49.3% and a high encapsulation efficiency of 98.6% were achieved. Furthermore, this nanoprecipitation approach can be adapted to produce stable drug-core polymer-shell nanoparticles with high drug loading (up to 58.5%) from a wide range of polymers and drugs (Figure 1c,d), including drugs from very hydrophobic to relatively hydrophilic such as paclitaxel (PTX), docetaxel (DTX), curcumin, amphotericin B, Scutellarin, Bulleyaconitine A, ibuprofen and ketamine; and various polymers including poly (D,L-lactide-co-glycolide)-block-poly(ethylene glycol) (PLGA-PEG) of different molecular weights, shellac, and poly(D,L-lactide)-*block*-poly(ethylene glycol) (PLA-PEG).

We argue that such drug-core polymer-shell nanoparticles with exceptionally high drug loading (near 50%) are generated as a result of the controlled sequential nanoprecipitation process using a solvent mixture instead of a single solvent. Figure 2a–e outlines the precipitation diagrams of curcumin and shellac in different solvents, showing the correlation between the amount of nanoparticles that precipitates out and the water/solvent volume ratio ($V_{water}/V_{solvent}$) considering the total number of nanoparticles when they precipitate out completely as 100%. When using the single solvent DMF, more than 80% of shellac precipitates when adding 1.6 times of water to the shellac-dissolved DMF solution ($V_w/V_s = 1.6:1$). However, curcumin only starts to precipitate at this volume ratio (Figure 2a3–5). The big difference in the precipitation volume ratio between shellac and curcumin (Figure 2a5) leads to the separate precipitation of shellac and curcumin nanoparticles thus big aggregates (Figure 2a2) and low drug loading using traditional single-solvent nanoprecipitation methods.

To determine the precipitation propensity of curcumin and shellac in different solvents, we dissolved them in different solvents, including EtOH, DMSO, and DMF. The solubility of shellac in these three solvents is EtOH > DMF > DMSO, while the solubility of curcumin is in the order of DMSO > DMF > EtOH. The basic idea is to use the precipitation curves of curcumin and shellac in DMF as the baseline and adjust the precipitation curves by increasing or decreasing DMSO or EtOH. For example, the ratio of DMSO can be increased to delay the precipitation of curcumin as it has a higher solubility in DMSO. To screen the anti-solvent, we used the precipitation curve to illustrate the mechanism of our sequential nanoprecipitation method.

To narrow down the gap between the two precipitation curves of curcumin and shellac (Figure 2a5) in single-solvent systems, two- or three-solvent mixtures with different volume ratios were screened. Compared to the single-solvent system, the two-solvent systems (DMF + EtOH) narrowed the gap

between the precipitation curves of curcumin and shellac (Figure 2b,c5) but the two curves still stayed apart from each other. As curcumin has the lowest solubility in EtOH among these three solvents, adding EtOH will result in faster precipitation of curcumin. In contrast, when the three-solvent system (DMF + EtOH + DMSO) was used, the precipitation curves of curcumin and shellac moved much closer (Figure 2d5) indicating that both the drug and polymer precipitate at a similar volume ratio. When a solvent mixture with DMSO/DMF/EtOH = 4:3:3 (v/v/v) was used, the encapsulation efficiency of curcumin increased to more than 90%. As shellac is more soluble in weak alkaline condition,[11] by using PBS or HEPES buffer at pH 7.4 we were able to precipitate curcumin first followed by shellac (Figure 2e3,4), so bring the curcumin curve to the left of the shellac curve (Figure 2e5). Consequently, the encapsulation efficiency increased further to 98.6% resulting in a very high drug loading of 49.3% (Figure 2e; Supporting Information, Figure S2). Because HEPES buffer contains a much lower concentration of salts than PBS buffer, the similar performance of these two buffers implied that pH, in this case, played a dominant role in controlling the encapsulation efficiency. To precipitate shellac completely, a minimum of 2.5 times of PBS or HEPES buffer needs to be added. After screening the long-term stability of NPs, the optimal anti-solvent/solvent ratio should fall within the range of 10:1 to 20:1 (v/v), to limit the Ostwald ripening effect as a result of the presence of the solvent in the solution.[12] Furthermore, we found this method is independent of mixing (Supporting Information, Figure S3), which is easy to understand as the precipitation in this case mainly depends on their intrinsic properties of solubility rather than mixing.

To show the versatility of this nanoprecipitation method, we produced various drug-loaded nanoparticles using different polymers, including PLGA, PLGA-PEG with different molecular weights, PLA-PEG, and different hydrophobic drugs, such as paclitaxel (PTX), docetaxel, ibuprofen, and ketamine. PLGA-PEG as an FDA approved polymer has been widely used to formulate various drug-loaded nanoparticles.[13] Both PLGA$_{10K}$-PEG$_{5K}$ and PLGA$_{55K}$-PEG$_{5K}$ polymers are soluble in DMSO and DMF but not in EtOH. We screened the optimal solvent formulation for making curcumin-loaded PLGA$_{10K}$-PEG$_{5K}$ NPs (10K-CUR). A maximum curcumin drug loading of 58.5% was achieved using a solvent mixture of DMSO, DMF and EtOH (3:3:4, v/v/v). Then we tried an anticancer drug, PTX, which has been regarded as one of the most difficult hydrophobic drugs to be encapsulated with high drug loading.[13b] Using our method, we successfully produced the PTX-core polymer-shell NPs using a similar tri-solvent formulation (DMSO/DMF/EtOH = 2:4:4, v/v/v) and PLGA$_{10K}$-PEG$_{5K}$ (10K-PTX). When the concentrations of PTX and PLGA$_{10K}$-PEG$_{5K}$ were 3 mg mL^{-1}, a drug loading of 49.1% was achieved. We also used the same tri-solvent system for PTX to encapsulate docetaxel (DTX), as DTX has a similar structure to PTX, and they both belong to the taxane class of drugs (Supporting Information, Figure S4).[14] The successful encapsulation of DTX using the same method as for encapsulating PTX suggests that we could encapsulate those drugs having similar
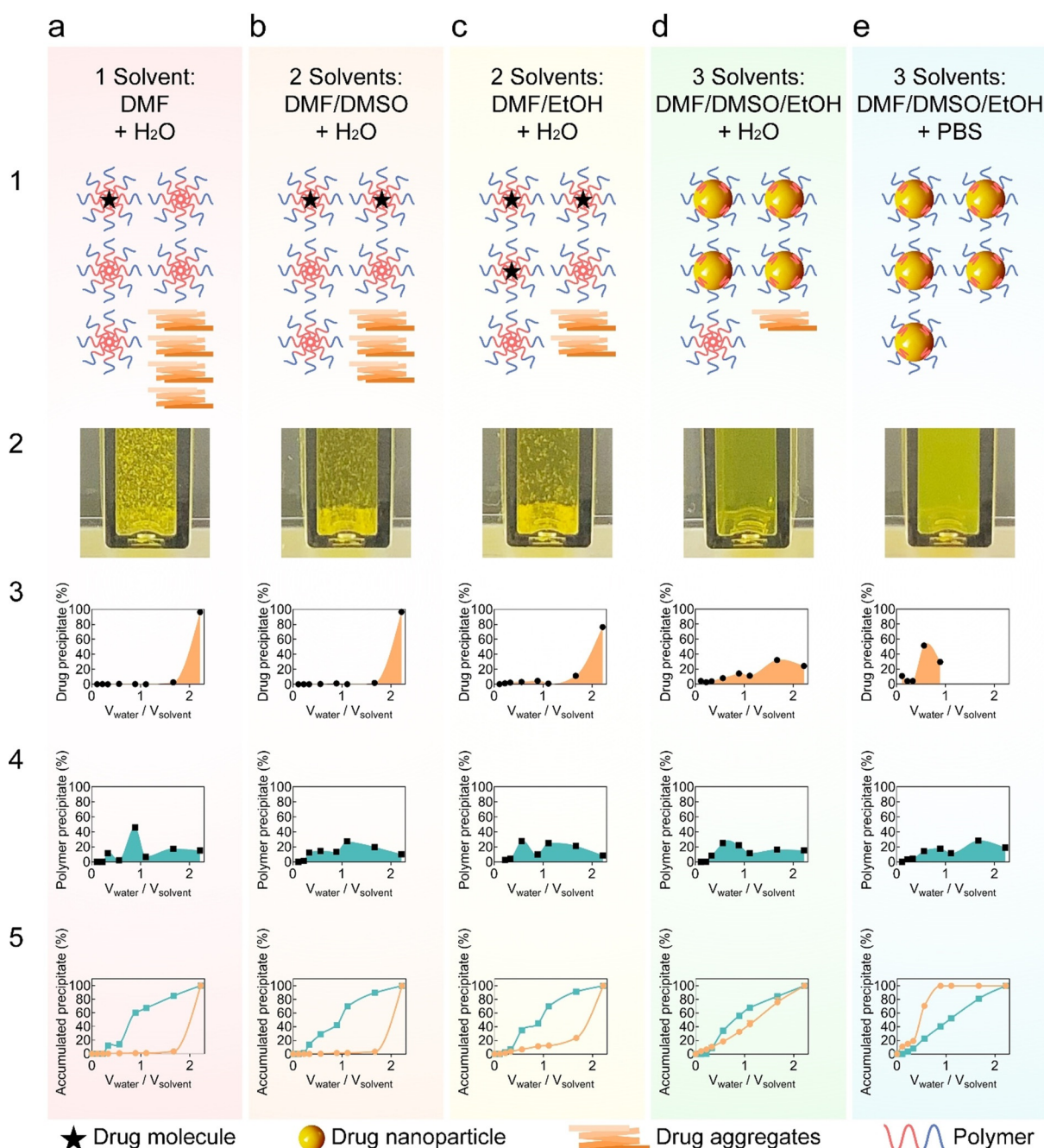
Figure 2. Nanoprecipitation of drug and polymer in one-, two-, and three-solvent formulations. The nanoprecipitation process of drug and polymer in a) a single-solvent system; b) two-solvent systems with DMF/DMSO (v/v = 1:1); and c) DMF/EtOH (v/v = 1:1); d),e) three-solvent system with DMSO/DMF/EtOH (v/v/v = 4:3:3) using d) water and e) PBS. The experimental schematic (**1**) and snapshot (**2**) showing the nanoparticle formation when adding 20 times of anti-solvent (water or buffer solution) to a solvent solution with a drug and polymer dissolved. (**3–5**) show the precipitation of drug (**3**), polymer (**4**), drug and polymer (**5**) when adding the anti-solvent repeatedly to the solvent solution containing either drug or polymer. For example, for the single solvent system, a drug and a polymer are dissolved in 180 μL DMF at the same concentration of 3 mg mL^{-1}, respectively. 20 μL water is added to the solution repeatedly. Considering the total amounts of nanoparticles when the drug or polymer completely precipitate out as 100%, the normalized drug precipitate (**3**) and polymer precipitate (**4**) against the total amount are shown as a function of the volume ratio of anti-solvent to solvent. (**5**) shows the accumulated precipitate curves of drug (yellow line) and polymer (blue line). Curcumin and shellac are used as the example system to demonstrate the nanoprecipitation process. The mean ± s.d. is from three independent replicates.

properties using the same method or with slight modification. We also successfully encapsulated amphotericin B, bulleya-conitine A, and scutellarin using the same tri-solvent system (DMSO:DMF:EtOH = 3:3:4, v/v/v) with drug loading rang-

ing from 43.8% to 49.1% (Supporting Information, Table S1 and Figure S4). To further validate our method, we also tested less hydrophobic drugs, such as ibuprofen and ketamine. We achieved drug loading of approximately 40% and encapsu-

lation efficiency of about 70% for ketamine due to its high water solubility. Moreover, we also encapsulated hydrophobic dye DiI in $PLGA_{10K\ or\ 55K}$-PEG_{5K} NPs with approximately 49% drug loading (DL) which have the potential applications in imaging.

It is critical to tune the drug release kinetics of drug-loaded nanoparticles. To allow programmed release, we re-engineer our nanoprecipitation process to form drug-core double-polymer nanoparticles. For example, by using two polymers with different degradation rates or swelling properties, the drug release kinetics can be controlled by tuning the ratio of the two polymers. We synthesized a list of nanoparticles with single or two polymers (Supporting Information, Table S1), including curcumin-core–shellac/$PLGA_{10K}$-PEG_{5K} double-polymer NPs (SH/10K-CUR; 10 K:SH = 1:1, w/w; DMSO:DMF:EtOH = 3:3:4, v/v/v) with 46.8% DL, PTX-core–shellac/$PLGA_{55K}$-PEG_{5K} NPs (SH/55K-PTX; SH:55K = 1:4, w/w; DMSO:DMF:EtOH = 2:4:4, v/v/v) with 39.6% DL, PTX-core $PLGA_{10-15K}$/$PLGA_{10K}$-PEG_{5K} NPs (10 K/PLGA-PTX; 10K:PLGA = 1:4, w/w; DMSO:DMF:EtOH = 2:4:4, v/v/v) with 35% DL, and PTX-core–shellac/$PLGA_{10K}$-PEG_{5K} NPs (SH/10K-PTX; SH:10K = 1:4, w/w; DMSO:DMF:EtOH = 2:4:4, v/v/v) with 37% DL (Supporting Information, Figure S5). The ratio of the two polymers can be tuned to control the release kinetics of the encapsulated drug.

Figure 3 shows the TEM images of different nanoparticles with high drug loading using our nanoprecipitation method. Three different morphologies were observed, namely, one drug-core in one NP (Figure 3a; Supporting Information, Figure S6), several drug NPs in the core (Figure 3b; Supporting Information, Figure S7), and many drug NPs in the core (Figure 3c). When the polymer precipitates straight away after a drug NP forms, one drug-core in one NP structure is formed. For example, when mixing curcumin and shellac in a solvent mixture (DMSO:DMF:EtOH = 4:3:3, v/v/v) with a buffer solution, monodispersed curcumin NPs of about 40 nm precipitated first followed by the immediate precipitation of shell covering the curcumin core forming the core–shell NPs of about 50 nm (Figure 3a). In contrast, when using the polymer $PLGA_{10K}$-PEG_{5K} to encapsulate curcumin, nanoparticles with several drug cores were observed as $PLGA_{10K}$-PEG_{5K} precipitates much slower than the drug (Figure 3b). Several drug NPs of 30–40 nm aggregated firstly followed by the precipitation of $PLGA_{10K}$-PEG_{5K} thus forming a core–shell nanoparticle containing several drug NPs in the core (Figure 3b). By adjusting the precipitation of the drug and polymer, core–shell nanoparticles with many drug NPs in the core were observed when using $PLGA_{55K}$-PEG_{5K} to encapsulate curcumin (Figure 3c).

Drug-loaded PLGA-PEG NPs such as 10K-CUR (Figure 3d,e; Supporting Information, Figure S8) and 55K-CUR (Figure 3f; Supporting Information, Figure S9) having several drug NPs (generally more than 5) inside one polymeric NP were bigger than the drug-loaded shellac NPs such as SH-CUR (Figure 3a) and SH-IBU (Figure 3g) due to the different precipitation time of polymers. Interestingly, the raspberry morphology of 55K-CUR NPs is very unique showing that many small curcumin NPs are encapsulated (Figure 3f). We

also synthesized PTX-loaded shellac/$PLGA_{55K}$-PEG_{5K} double-polymer NPs (SH/55K-PTX, Figure 3h and Figure S10) and curcumin loaded double-polymer NPs (SH/10K-CUR, Figure 3i) showing a similar spherical structure. High-resolution TEM and electron diffraction patterns demonstrated the amorphous structure of the PTX-loaded shellac/$PLGA_{55K}$-PEG_{5K} double-polymer NPs, which is beneficial as the drug solubility can be improved (Supporting Information, Figure S11).[15]

One of the major challenges to making nanoparticles with high drug loading is the high propensity toward aggregation during storage. We examined the stability and release kinetics of curcumin-loaded NPs (Figure 4a,b) including curcumin-loaded single-polymer NPs (SH-CUR and 10K-CUR), and curcumin-loaded double-polymer NPs (SH/10K-CUR) with various polymer ratios (SH:10K = 5:1, 2:1, and 1:1, w/w) in PBS (Figure 4a; Supporting Information, Figure S12). We noticed that NP sizes changed more significantly with more shellac, because shellac is stable in acidic condition (Supporting Information, Figure S13) but swells and gradually dissolves in PBS.[11] Based on this property of shellac, we could tune the release profile of the drug-loaded polymer NPs by changing the shellac ratios in the polymer shell. We next evaluated the release profiles of curcumin-loaded single and double-polymer formulations in PBS containing 0.5% w/v Tween 80 under 37°C with gentle shaking (Figure 4b). The single-polymer formulation (SH-CUR) exhibited a fast release kinetics in the first 24 hours, then a more sustained release. In contrast, the release profile of the double-polymer formulation (SH/10K-CUR) showed a sustained release over seven days (Figure 4b). The TEM images show that the single-polymer formulation SH-CUR swelled and released a significant amount of drugs (dark particles) after 24 hours (Figure 4c). In contrast, the double-polymer formulation SH/10K-CUR showed very minimum drug release and their morphology remained unchanged after 24 hours (Figure 4d).

We also tested the stability and release profile of PTX-loaded NPs (Figure 4e,f). For the short-term stability of the PTX-loaded double-polymer NPs in PBS for 21 days, the polymer ratio of shellac to $PLGA_{10K/55K}$-PEG_{5K} was kept at 1:4 (w/w) for the SH/55K-PTX and SH/10K-PTX NPs. Due to the higher propensity of PTX to precipitate and aggregate than curcumin, the PTX loaded single-polymer NPs can only be stable for several hours. However, all the double-polymer formulations were remarkably stable for the time course of our experiments (21 days) (Figure 4e). The release profiles of the PTX-loaded double-polymer formulation (SH/55K-PTX) was distinct showing a sustained release over seven days (Figure 4f). Moreover, the SH/55K-PTX NPs showed good stability in serum over 48 hours incubation under 37°C (Supporting Information, Figure S14). For future clinical applications, the shelf-life of the nanoparticle product is critical. We evaluated the long-term stability of the lyophilized SH/55K-PTX NPs (39.6% DL) (Figure 4g). Even after 15 months storage, the NP powder can be easily resuspended with gentle shaking or vortex (Figure 4h). The recovered nanosuspension had the same size (ca. 100 nm) and PDI (ca. 0.2) as the freshly prepared nanosuspension after 15-month storage with high retention of PTX ($\geq$ 94.8%).
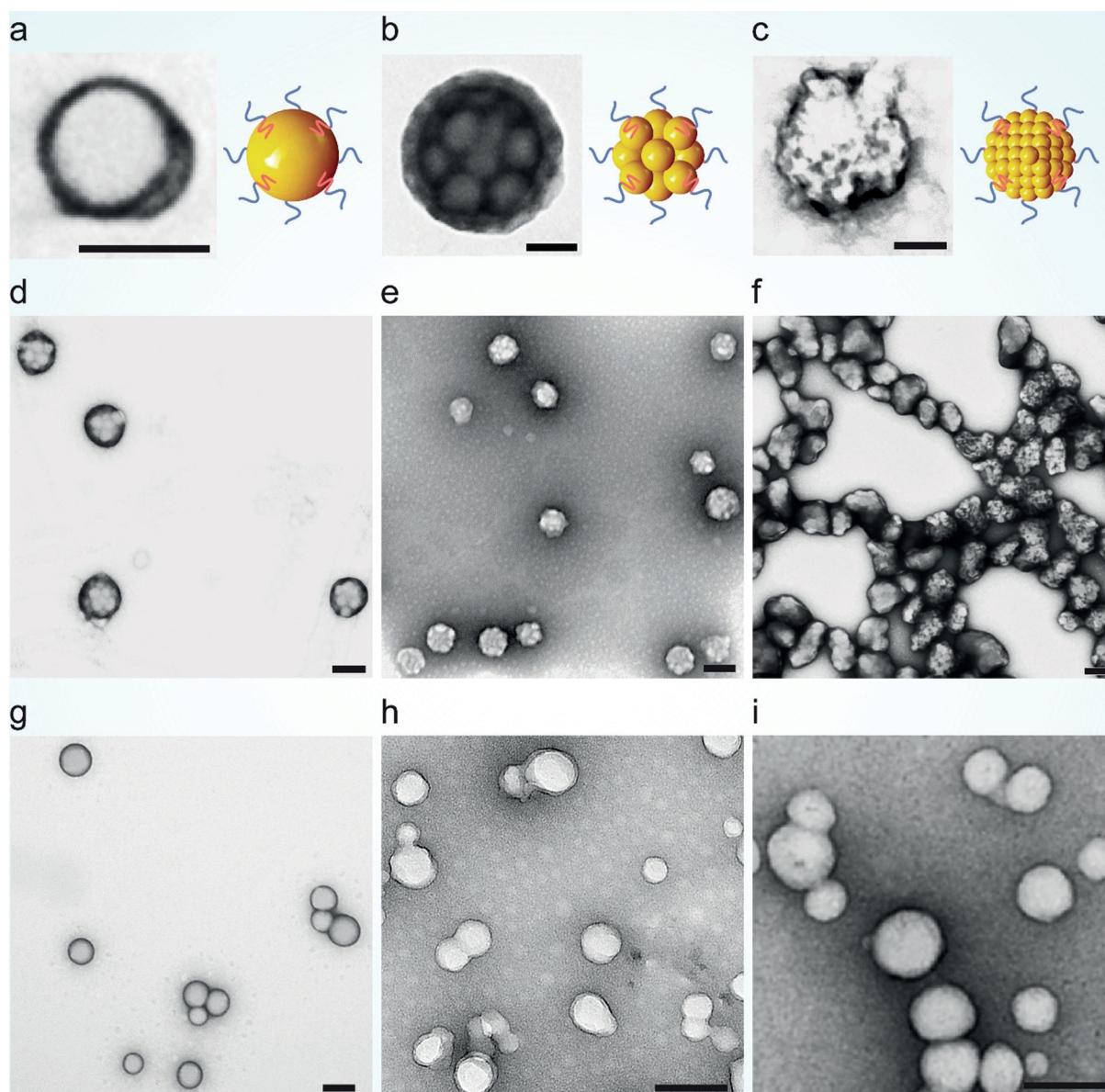
Figure 3. Illustration and TEM images of nanoparticles with high drug loading (DL) using our nanoprecipitation method. Three morphologies were observed, namely, a) one drug-core in one NP, b) multiple drug NPs in the core, and c) plentiful drug NPs in the core. a) Single particle image of curcumin-loaded shellac NPs (SH-CUR; DL: 49.3%). b) Single particle image of curcumin-loaded $PLGA_{10K}$-PEG_{5K} NPs (10K-CUR; DL: 45.5%). c) Single particle image of curcumin-loaded $PLGA_{55K}$-PEG_{5K} NPs (55K-CUR; DL: 49.5%). d) TEM image of curcumin-loaded $PLGA_{10K}$-PEG_{5K} NPs (10K-CUR; DL: 45.5%), e) TEM image of curcumin-loaded $PLGA_{10K}$-PEG_{5K} NPs with highest drug loading (10K-CUR_{max}; DL: 58.5%) and f) curcumin-loaded $PLGA_{55K}$-PEG_{5K} NPs (55K-CUR; DL: 49.5%). g) TEM image of ibuprofen-loaded shellac NPs (SH-IBU; DL: 38%). h) TEM image of PTX-loaded double-polymer shellac/$PLGA_{55K}$-PEG_{5K} NPs (SH/55 K -PTX; DL: 39.6%). i) TEM image of curcumin-loaded double-polymer shellac/$PLGA_{10K}$-PEG_{5K} NPs (SH/10K-CUR; DL: 46.8%). Scale bars: 50 nm for (a)–(c) and 100 nm for (d)–(i).

It is evident that the increase of drug loading of drug-loaded nanoparticles can reduce the material used when using the same dose of a drug which is more economic and may have fewer side effects caused by the toxicity of the excess nanoparticle materials.[16] Nevertheless, to evaluate whether nanoparticles with a high drug loading have any additional therapeutic advantages over nanoparticles with low drug loading, we synthesized two types of nanoparticles, namely, PTX-loaded double-polymer nanoparticles (shellac and $PLGA_{55K}$-PEG_{5K} at a mass ratio of 1:4) with high drug loading (39.6%) and low drug loading (3.5%). Using these

two type of nanoparticles, we investigated their cell cytotoxicity using 2D cell monolayer and 3D tumor spheroid in vitro models. The PTX-loaded NPs with high drug loading illustrated reduced cell viability compared to the nanoparticles with low drug loading in both 2D-monolayer cells (Figure 5a) and 3D-tumor spheroids at the same drug concentration (Figure 5b). Additionally, we also investigated the growth curve of the tumor spheroid incubated with PTX-loaded NPs with high and low drug loading. Compared to the spheroids treated with free PTX and low drug loading NPs, those treated with the high drug loading NPs exhibit
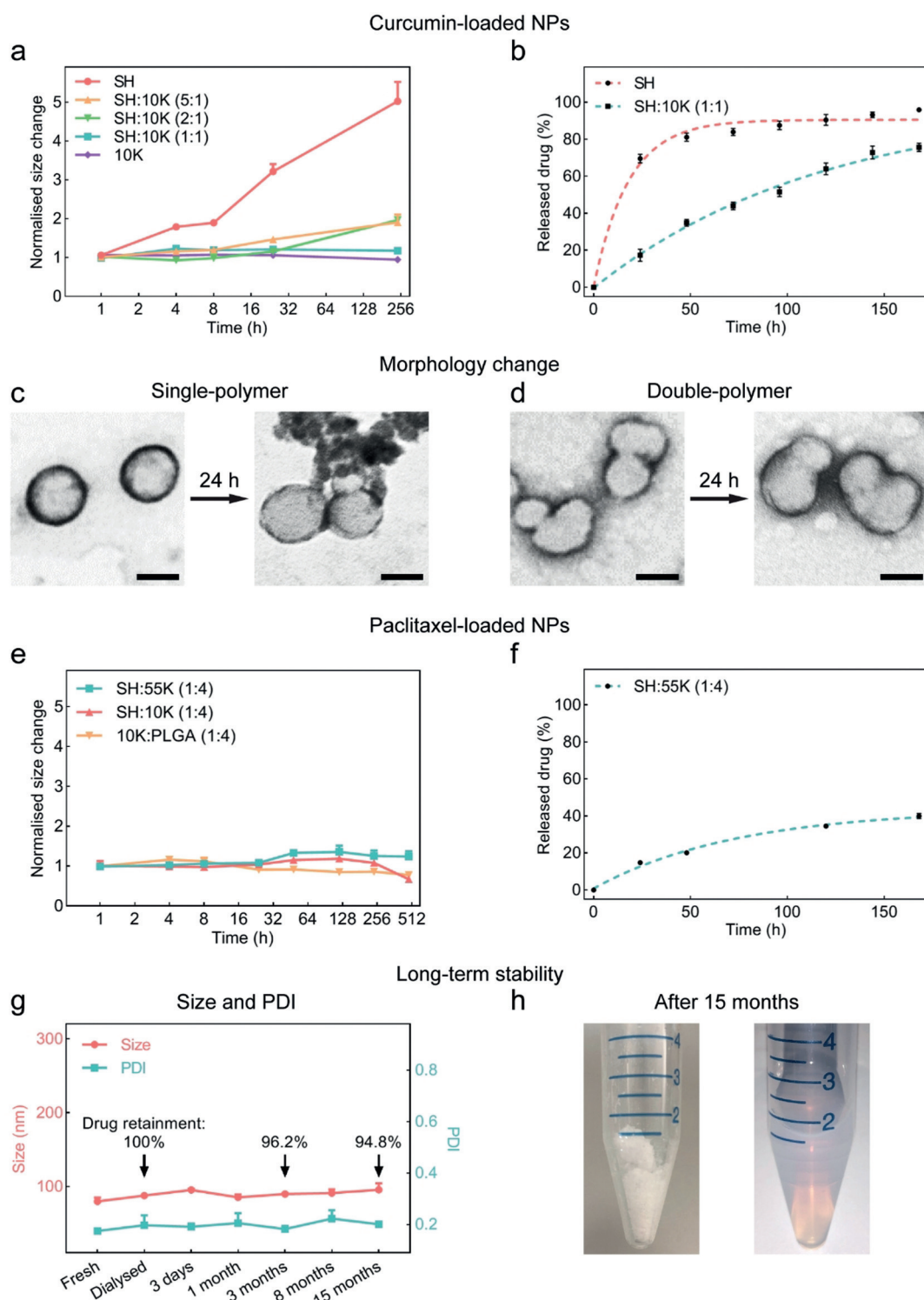
Figure 4. Stability and release profiles of curcumin and PTX-loaded single and double-polymer formulations in PBS. a) Stability test of curcumin-loaded NPs: curcumin-loaded shellac NPs (SH-CUR), curcumin-loaded PLGA$_{10K}$-PEG$_{5K}$ NPs (10K-CUR) and curcumin-loaded double-polymer shellac/PLGA$_{10K}$-PEG$_{5K}$ NPs (SH/10K-CUR) with SH:10 K ratio (w/w) of 5:1, 2:1 and 1:1. b) Release profiles of SH-CUR and SH/10 K (1:1)-CUR. The release was conducted in PBS containing 0.5% w/v Tween 80 under 37°C with gentle shaking. TEM images of c) curcumin-loaded single-polymer formulation (SH) and d) double-polymer formulation (SH:10K(1:1)) after 0 and 24 hours of incubation in PBS under 37°C with 100 rpm shaking. Scale bar: 50 nm. e) The stability test of paclitaxel (PTX)-loaded double-polymer NPs: PTX-loaded shellac/PLGA$_{55K}$-PEG$_{5K}$ NPs (SH:55 K (1:4)), PTX-loaded shellac/PLGA$_{10K}$-PEG$_{5K}$ NPs (SH:10 K (1:4)) and PTX-loaded PLGA$_{10-15K}$/PLGA$_{10K}$-PEG$_{5K}$ NPs (10 K:PLGA (1:4)). f) Release profiles of PTX-loaded shellac/PLGA$_{55K}$-PEG$_{5K}$ NPs (SH:55 K (1:4)). The release was conducted in PBS containing 0.5% w/v Tween 80 under 37°C with gentle shaking. g) Long-term stability test of lyophilized PTX-loaded shellac/PLGA$_{55K}$-PEG$_{5K}$ NPs (SH:55 K (1:4)) and h) snapshots of its dry powder and the resuspended solution after 15-month storage under −20°C. The mean ± s.d. from three independent replicates is shown for (a), (b), (e), (f), and (g).
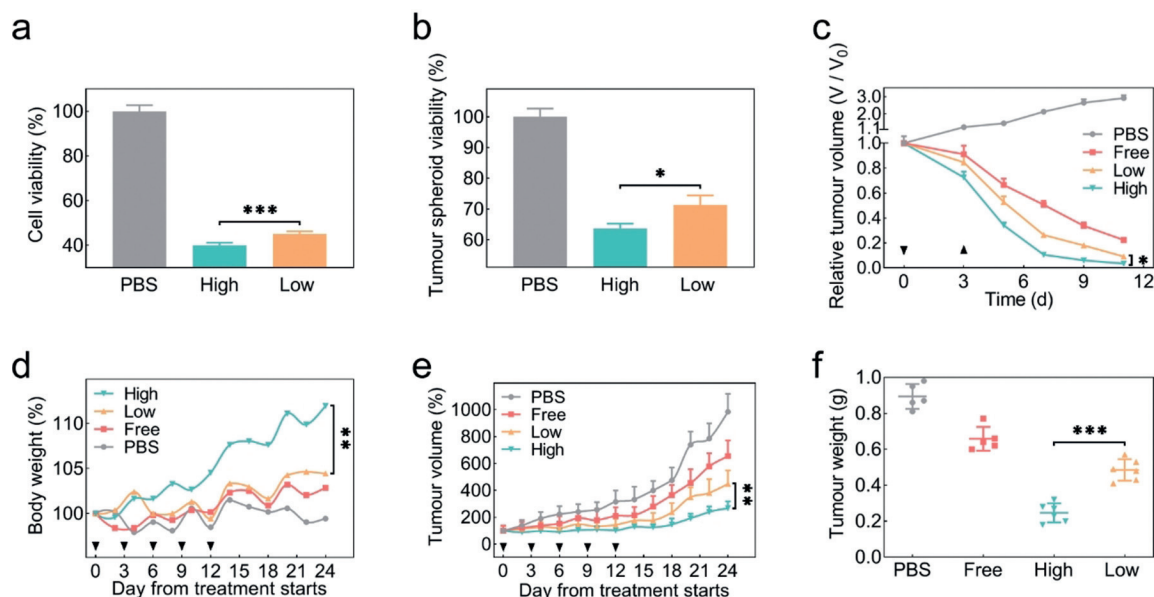
Figure 5. In vitro and in vivo anti-tumor effects of PTX-loaded high- (SH/55K-PTX; DL: 39.6%) (High DL NP) and low-drug loading formulations (SH/55K-PTX; DL: 3.5%) (Low DL NP). a) Cytotoxicity of 2D cells for High and Low DL NP (48 h, 0.9 µg mL^{-1} PTX); b) Cytotoxicity of the High and Low DL NP for SKOV3 tumor spheroids (72 h, 0.1 µg mL^{-1} PTX); * and *** represent statistically significant difference $p < 0.05$ and 0.001, respectively (mean ± SD; $n = 3$ per group for a and b). c) The tumor spheroid growth curve after incubation of the PBS, Free PTX, High and Low DL NP for 72 h (0.1 µg mL^{-1} PTX). Day 0 is the day of adding Free PTX and PTX-loaded NPs while Day 3 is the starting date of gradual drug removal by replacing 50% of the total medium every 48 h. * represent statistically significant difference $p < 0.05$ (mean ± SD; $n = 5$ per group). d) Body weight and e) tumor volume of tumor-bearing mice during 24 days since 1st injection (Day 0) for PBS, Free PTX, High and Low DL NP groups. Five injections in total at day 0, 3, 6, 9 and 12. f) Tumor weight of isolated tumors from tumor-bearing mice after treatment of PBS, Free PTX, Low and High DL NP. ** and *** represent statistically significant difference $p < 0.01$ and 0.001, respectively (mean ± SD; $n = 6$ per group for d, e, and f).

persistent volume decrease, indicating its significant anti-tumor effect (Figure 5 c).

We further studied the in vivo anti-tumor therapeutic effects of PTX-loaded high- (SH/55 K -PTX; DL: 39.6%) (High DL NP) and low-drug loading formulations (SH/55K-PTX; DL: 3.5%) (Low DL NP) in tumor-bearing mice. After initial tumor establishment, four formulations (PBS, Free PTX, High DL NP, and Low DL NP) were intravenously injected into the mice at every 72 hours for five injections in total. The body weight and tumor volume growth curves are displayed in Figure 5 d,e, respectively. The body weight of the mice treated with High DL NP increased (12.0% increase at day 25) faster than Low DL NP group (4.4% increase at day 25) and Free PTX group (2.9% increase at day 25). In addition, the tumor volume of High DL NP group grew significantly slower than the other groups, at day 24 post-injection the tumor volume of PBS, Free PTX, Low DL NP, and High DL NP groups increased 885.0%, 556.0%, 347.8%, and 167.6%, respectively. The High DL NP showed enhanced tumor inhibition effect than the Low DL NP and Free PTX at the same drug dosage (Figure 5 f; Supporting Information, Figure S15). Additionally, the nanoparticle concentration in the High DL NP is much lower than the Low DL NP (Supporting Information, Figure S16), which offers some advantages in terms of intravenous injection, large scale production of such polymer NPs and production cost as well. The histopathological analysis of tumor and main organs (Supporting Information, Figure S17) shows that the High DL NP group has the most tumor tissue necrosis but no obvious

necrosis or cell death in major organs including liver, spleen, kidney, heart, lung, and brain. Our preliminary in vivo results demonstrated some advantages of using the High DL NP formulation over the Low DL NP in terms of efficacy and safety (Supporting Information, Figure S18). More studies including PK/PD, biodistribution, dosing, dosing schedule, and different mice models will be conducted in future.

Conclusion

The controlled synthesis of drug-core polymer-shell nano-composites with an exceptionally high drug loading (up to 58.5% w$_{drug}$/w$_{drug+polymer}$) and high encapsulation efficiency (up to 98.5%) was achieved using a sequential nanoprecipitation method. This platform technology is based on controlling the sequential precipitation of the drug and polymer using an organic solvent system comprising two or more organic solvents. This allows the precipitation of the drug preferably just prior to the precipitation of the polymer. More importantly, we demonstrated the versatility of this technology to encapsulate various hydrophobic molecules, such as paclitaxel, curcumin, and ibuprofen. According to our in vitro and in vivo results, the high-drug-loading NPs synthesized using our technology demonstrated an enhanced therapeutic effect and improved safety. Additionally, our high-drug-loaded NPs can achieve long-term stability (> 15 months) after lyophilisation, demonstrating their potential for future clinical applications. In future scale-up production of nanoparticles

using nanoprecipitation, how to minimize the use of organic solvents and how to recycle the solvents should be carefully engineered. Nevertheless, this technology offers a new strategy for the manufacture of polymeric nanoparticles with high drug loading and opens unique opportunities for drug encapsulation and drug delivery applications.

Conflict of interest

The authors declare the following competing interests: The University of Queensland (UQ) filed a patent on the core-shell polymer nanoparticles (PCT/AU2019/050557, filed 31 May 2019). Y.L., G.Y., T.B. and C.-X.Z. are named inventors on this patent and through their employment with UQ hold an indirect interest in this intellectual property. The other authors declare no competing interest.

[1] a) V. P. Torchilin, *Nat. Rev. Drug Discovery* **2014**, *13*, 813; b) K. S. Soppimath, T. M. Aminabhavi, A. R. Kulkarni, W. E. Rudzinski, *J. Controlled Release* **2001**, *70*, 1–20; c) M. Liong, J. Lu, M. Kovochich, T. Xia, S. G. Ruehm, A. E. Nel, F. Tamanoi, J. I. Zink, *ACS Nano* **2008**, *2*, 889–896; d) K. M. Wasan, D. R. Brocks, S. D. Lee, K. Sachs-Barrable, S. J. Thornton, *Nat. Rev. Drug Discovery* **2008**, *7*, 84; e) V. P. Torchilin, *Nat. Rev. Drug Discovery* **2005**, *4*, 145.

[2] J. Panyam, V. Labhasetwar, *Adv. Drug Delivery Rev.* **2003**, *55*, 329–347.

[3] a) Z. Liu, Y. Jiao, Y. Wang, C. Zhou, Z. Zhang, *Adv. Drug Delivery Rev.* **2008**, *60*, 1650–1662; b) P. Couvreur, *Adv. Drug Delivery Rev.* **2013**, *65*, 21–23; c) G. A. Husseini, W. G. Pitt, *Adv. Drug Delivery Rev.* **2008**, *60*, 1137–1152; d) L. Zhang, J. M. Chan, F. X. Gu, J.-W. Rhee, A. Z. Wang, A. F. Radovic-Moreno, F. Alexis, R. Langer, O. C. Farokhzad, *ACS Nano* **2008**, *2*, 1696–1702.

[4] a) H. Zhang, D. Wang, R. Butler, N. L. Campbell, J. Long, B. Tan, D. J. Duncalf, A. J. Foster, A. Hopkinson, D. Taylor, *Nat. Nanotechnol.* **2008**, *3*, 506; b) M. Giardiello, N. J. Liptrott, T. O. McDonald, D. Moss, M. Siccardi, P. Martin, D. Smith, R. Gurjar, S. P. Rannard, A. Owen, *Nat. Commun.* **2016**, *7*, 13184; c) J. J. Hobson, P. Curley, A. C. Savage, A. Al-khouja, M. Siccardi, C. Flexner, C. F. Meyers, A. Owen, S. P. Rannard, *Nanoscale Adv.* **2019**, *1*, 4301–4307.

[5] R. Ran, Q. Sun, T. Baby, D. Wibowo, A. P. Middelberg, C.-X. Zhao, *Chem. Eng. Sci.* **2017**, *169*, 78–96.

[6] a) J. Hrkach, D. Von Hoff, M. M. Ali, E. Andrianova, J. Auer, T. Campbell, D. De Witt, M. Figa, M. Figueiredo, A. Horhota, *Sci. Transl. Med.* **2012**, *4*, 128ra39; b) Y. Matsumura, *Adv. Drug Delivery Rev.* **2008**, *60*, 899–914; c) K.-J. Chen, L. Tang, M. A. Garcia, H. Wang, H. Lu, W.-Y. Lin, S. Hou, Q. Yin, C. K.-F. Shen, J. Cheng, *Biomaterials* **2012**, *33*, 1162–1169; d) J. Cheng, B. A. Teply, I. Sherifi, J. Sung, G. Luther, F. X. Gu, E. Levy-Nissenbaum, A. F. Radovic-Moreno, R. Langer, O. C. Farokhzad, *Biomaterials* **2007**, *28*, 869–876; e) J. Xu, Q. Zhao, Y. Jin, L. Qiu, *Nanomedicine* **2014**, *10*, 349–358.

[7] a) D. Liu, H. Zhang, S. Cito, J. Fan, E. Mäkilä, J. Salonen, J. Hirvonen, T. M. Sikanen, D. A. Weitz, H. A. Santos, *Nano Lett.* **2017**, *17*, 606–614; b) K. Cai, X. He, Z. Song, Q. Yin, Y. Zhang, F. M. Uckun, C. Jiang, J. Cheng, *J. Am. Chem. Soc.* **2015**, *137*, 3458–3461; c) S. Lv, Y. Wu, K. Cai, H. He, Y. Li, M. Lan, X. Chen, J. Cheng, L. Yin, *J. Am. Chem. Soc.* **2018**, *140*, 1235–1238.

[8] a) J. Tao, S. F. Chow, Y. Zheng, *Acta Pharm. Sin. B* **2019**, *9*, 4–18; b) R. F. Pagels, J. Edelstein, C. Tang, R. K. Prud'homme, *Nano Lett.* **2018**, *18*, 1139–1144; c) K. M. Pustulka, A. R. Wohl, H. S. Lee, A. R. Michel, J. Han, T. R. Hoye, A. V. McCormick, J. Panyam, C. W. Macosko, *Mol. Pharm.* **2013**, *10*, 4367–4377.

[9] a) Y. Liu, C. Cheng, R. K. Prud'homme, R. O. Fox, *Chem. Eng. Sci.* **2008**, *63*, 2829–2842; b) B. K. Johnson, R. K. Prud'homme, *AIChE J.* **2003**, *49*, 2264–2282.

[10] a) D. Chen, C.-X. Zhao, C. Lagoin, M. Hai, L. R. Arriaga, S. Koehler, A. Abbaspourrad, D. A. Weitz, *R. Soc. Open Sci.* **2017**, *4*, 170919; b) C. Coelho, R. Nanabala, M. Ménager, S. Commereuc, V. Verney, *Polym. Degrad. Stab.* **2012**, *97*, 936–940.

[11] A. Patel, P. Heussen, J. Hazekamp, K. P. Velikov, *Soft Matter* **2011**, *7*, 8549–8555.

[12] a) P. W. Voorhees, *J. Stat. Phys.* **1985**, *38*, 231–252; b) Y. Liu, K. Kathan, W. Saad, R. K. Prud'homme, *Phys. Rev. Lett.* **2007**, *98*, 036102.

[13] a) Y. Liu, Y. Hui, R. Ran, G. Z. Yang, D. Wibowo, H. F. Wang, A. P. Middelberg, C. X. Zhao, *Adv. Healthcare Mater.* **2018**, *7*, 1800106; b) A. Kumari, S. K. Yadav, S. C. Yadav, *Colloids Surf. B* **2010**, *75*, 1–18; c) R. A. Jain, *Biomaterials* **2000**, *21*, 2475–2490.

[14] P. A. Vasey, G. C. Jayson, A. Gordon, H. Gabra, R. Coleman, R. Atkinson, D. Parkin, J. Paul, A. Hay, S. B. Kaye, *J. Natl. Cancer Inst.* **2004**, *96*, 1682–1691.

[15] E. Amstad, M. Gopinadhan, C. Holtze, C. O. Osuji, M. P. Brenner, F. Spaepen, D. A. Weitz, *Science* **2015**, *349*, 956–960.

[16] A. Nel, T. Xia, L. Mädler, N. Li, *Science* **2006**, *311*, 622–627.